Hindawi
Journal of Nanotechnology
Volume 2020, Article ID 3139701, 9 pages
https://doi.org/10.1155/2020/3139701

Research Article

Synthesis of Specific ZnF Based Nanoparticles ($ZnFe_2O_4$): Antimicrobial Properties, Surface Characteristics, and Adsorption Activity for AB 29 Textile Dye

Ferda Gönen and Gökhan Tekinerdoğan

Mersin University, Chemical Engineering Department, Mersin 33343, Turkey

Correspondence should be addressed to Ferda Gönen; gonenf74@gmail.com

Received 16 September 2019; Accepted 14 February 2020; Published 2 July 2020

Guest Editor: Giorgio Vilardi

In this investigation, the color removal from synthetic wastewaters containing Acid Blue 29 (AB 29) dye was investigated by ZnF-based nanomaterials ($ZnFe_2O_4$) synthesized by the coprecipitation method in a batch system. SEM, FT–IR, and XRD analysis were used for the characterization of the nanoparticles (before and after adsorption), and the analysis results were compared with each other. The parameters such as pH, temperature, dye concentration, and nanoparticle dosage affecting color removal were examined systematically, and favorable color removal conditions were determined by the classical approach. From the experimental results, the favorable conditions with high removal efficiency for the adsorption were determined: removal temperature 35°C and the removal pH 2.0. At these experimental conditions, the adsorbed dye amount per unit mass of adsorbent and the percentage dye removal were determined as 1489.79 $mg{\cdot}g^{-1}$ and 98.83%, respectively. In the other part of the research, three different isotherm models (Langmuir, Freundlich, and Temkin) were used to examine the adsorption equilibrium data. Langmuir and especially Freundlich linear isotherm models provided the highest R^2 regression coefficients, successfully. The kinetic data was evaluated by pseudo-first-order and pseudo-second-order kinetic model approach. It was observed that pseudo-second-order kinetic model best represented AB 29-ZnF adsorption kinetic data. The determined thermodynamic parameters such as ΔH, ΔS, and ΔG were proved that the AB 29-ZnF adsorption system was an exothermic ($\Delta H < 0$), spontaneous, thermodynamically favorable ($\Delta G < 0$), and stabilized system without any structural changes in sorbate and sorbents ($\Delta S<0$).

1. Introduction

The color caused by domestic and industrial pollution sources is undesirable for the aesthetic appearance of water [1, 2]. Also the discharge of textile industry wastewaters including large amount of azo dyes having nonbiodegradability, toxicity, and carcinogenic properties poses a major threat to the ecosystem and especially aquatic life depending on their high concentration and stability in wastewaters [3, 4]. Reactive dyestuffs are an important class of commercially important textile dyestuffs. On the other hand, these reactive dyestuffs are one of the most stable and polluting dyestuffs during the dyeing process. Reactive dyes exhausted are about 50% in their hydrolysed and unfixed form during the washing process, and treatment of them is problematic [5–7].

Physical, chemical, and biological treatment methods are presently used for textile wastewater treatment. These methods are osmosis, chlorination, ozonation, filtration, oxidation processes, nanofiltration, chemical precipitation, ion exchange, and chemical coagulation/flocculation. The conventional biological treatment methods may not provide adequate treatment for the complete color removal and degradation of organics and dyes. Physical/physicochemical methods such as coagulation and ion exchange are not frequently preferred for wastewater treatment because of high operational costs. Chlorination and ozonation processes cause degradation by chemical reaction and allow breaking down harmful large into smaller ones. Moreover, discharching chlorinated compounds to the environment causes some serious environmental problems. Also,

ozonation is an unstable process and requires large capital expenses depending on the need for immediate use for rapid chemical process. Many researchers have investigated water treatment containing color removal by adsorption using low cost and environmentally compatible materials [8–10]. When investigations conducted in recent years are examined, there is a limited number of investigations using magnetic, antimicrobial, and suitable for more than one application especially for color removal from wastewaters containing chemical and biological pollution load. In this investigation, the synthetically prepared wastewater solutions containing AB 29 dye were examined for the color removal by ZnF-based nanoparticle. The novelty of this research is the use of ZnF-based nanomaterial with superior advantages such as low cost, antimicrobial, and environmentalist characteristics in treatment of textile dye solution. The most important advantages of ZnF-based nanomaterials is antimicrobial property to many harmful pathogens. So, this investigation proved the removal of two different types of pollutant load (biological and chemical) in domestic and/or industrial wastewater with high efficiency by using only one novel adsorbent, $ZnFe_2O_4$.

2. Experiments

2.1. Reagents. In order to synthesize the zinc oxide ($ZnFe_2O_4$) nanoparticles, Iron (III) chloride ($FeCl_3$), zinc chloride ($ZnCl_2$), sodium hydroxide (NaOH), and hydrochloric acid (HCl) reagents were obtained from Merck. Moreover, AB 29 dye was obtained from Sigma-Aldrich.

Bacillus subtilis, *Klebsiella pneumoniae*, *Escherichia coli*, and *Enterococcus fecalis* bacteria obtained from Mersin University Microbiology Laboratory of the Biology Department were used during the investigation of antimicrobial effect of ZnF-based adsorbent.

2.2. Synthesis of Nanoparticles. ZnF-based nanomaterials were synthesized by the coprecipitation method for the adsorption of AB 29 dye solution. 200 mL of 0.75 M Iron (III) chloride ($FeCl_3$) and 200 mL of 0.25 M zinc chloride ($ZnCl_2$) solutions were mixed with each other, and then the solution was stirred. After that, 2 M NaOH solution was added to this mixture while the pH value was 10 in a magnetic stirrer at 60°C. The final solution was filtered at 60°C for 18 hours. The drained solution was calcined in an ash oven at 300°C, and the synthesized particles were converted into powdered particles in the mortar [11].

2.3. Characterization Experiments. FTIR (Perkin Elmer, Fourier Transform Infrared Spectrometer), SEM (ZeissSupra 55 Area Emission, Scanned Electron Microscope), and XRD (Philips, X'Pert brand X-ray Diffractometer) were used for identification of morphological properties and identification of phases and crystal structures of synthesized particles at Mersin University Advanced Materials Research Center (MEITAM).

2.4. Color Removal Experiments. Color removal experiments were carried out at 120 rpm constant agitation rate in a batch system. Desired amount of FeZn-based nanoparticles were weighed and then mixed with 150 mL dye solutions (AB 29) adjusted to the desired pH values with NaOH and HCl solutions. Samples were taken and centrifuged at specific time intervals (0, 5, 15, 30, 60, 120, 180, 240, 300, 360, 420, 1440, 1500, 1600, 1800, and 2000) in the shaking water bath. Centrifuged samples were diluted and analyzed by using a UV-Vis spectrophotometer at 663 nm wavelength. Dye removal % was determined by the following formula:

$$\text{Dye Removal \%} = \left(\frac{C_0 - C_e}{C_0}\right) \times 100, \quad (1)$$

where C_0 and C_e are the initial and equilibrium dye concetration in $mg{\cdot}L^{-1}$, respectively. The amount of dye adsorbed per unit of the adsorbent at equilibrium was calculated in terms of q_e ($mg{\cdot}g^{-1}$) using the equation given below. The equilibrium amount of dye removal per unit of the nanoparticle was determined in terms of q_e ($mg{\cdot}g^{-1}$) using the following equation.

$$\text{Removal capacity}\,(q_e) = \frac{(C_0 - C_e)V}{m}, \quad (2)$$

where V is the volume of dye solution (L) and m is the mass of the adsorbent (g).

2.5. Microorganism Growth and Storage Conditions Used for Determination of Antimicrobial Activity of Nanoparticle. *Bacillus subtilis*, *Klebsiella pneumoniae*, *Escherichia coli*, and *Enterococcus fecalis* bacteria used in determination of the antimicrobial effect of nanoparticle were kindly supplied from Dr. AO Adıgüzel, Faculty of Science, Biology Department, Mersin University, Turkey. For the cultivation, Nutrient Agar Nutrient (NA) and Eosin Methylene-blue lactose sucrose agar (EMB) media were used.

2.6. Determination of Antimicrobial Effect of the Nanoparticle. The diffusion method was used to determine the antimicrobial effect of bacterial cultures. Mueller–Hinton Agar (MHA) was used as a nutrient in this method based on the inhibition of the development of microorganisms in the field where the substance to be tested is diffused in the agar. In this method, at the end of the incubation period, ZnF ($ZnFe_2O_4$) based nanomaterials were added to the open zone (microorganism cannot develop) formation around the holes. The resulting zone diameters were measured in mm. The standard deviation of zone diameters was calculated by performing all tests in 3 repetitions. [10–13].

3. Results and Discussion

3.1. Characterization Studies for ZnF-Based Nanoparticles

3.1.1. SEM Results. SEM analyzes were carried out to determine the morphological characteristics of ZnF-based adsorbent before and after AB 29 dye adsorption. SEM images shown in Figure 1 demonstrate that the synthesized

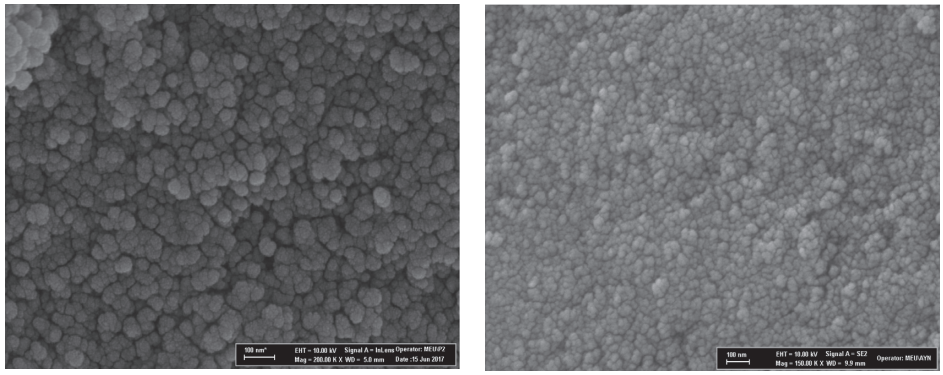

(a) (b)

Figure 1: SEM images for ZnF-based adsorbent (a) before adsorption (b) after adsorption.

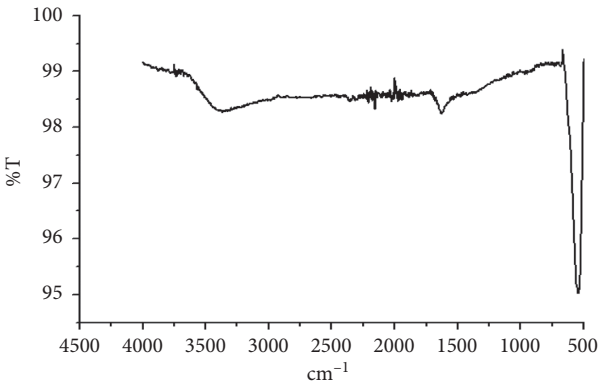

Figure 2: FT-IR spectrum of ZnF-based adsorbent before AB 29 dye adsorption.

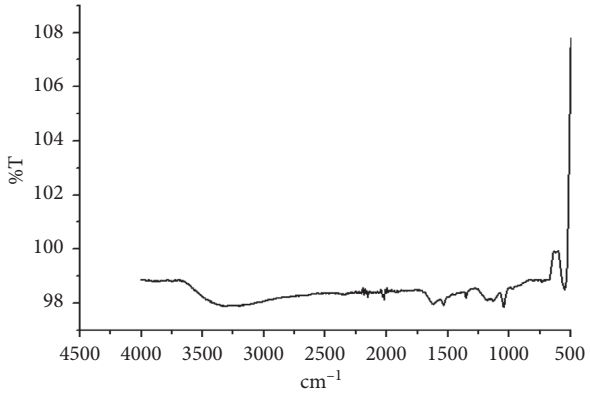

Figure 3: FT-IR spectrum of ZnF-based adsorbent after AB 29 dye adsorption.

material has a bulk structure. It is observed that there are many macropores on the surface of the ZnF-based nanoparticles supplying an evidence about efficient use as an adsorbent.

As it seen from the obtained SEM images, the pores were filled and the surface was filled with dye molecules after

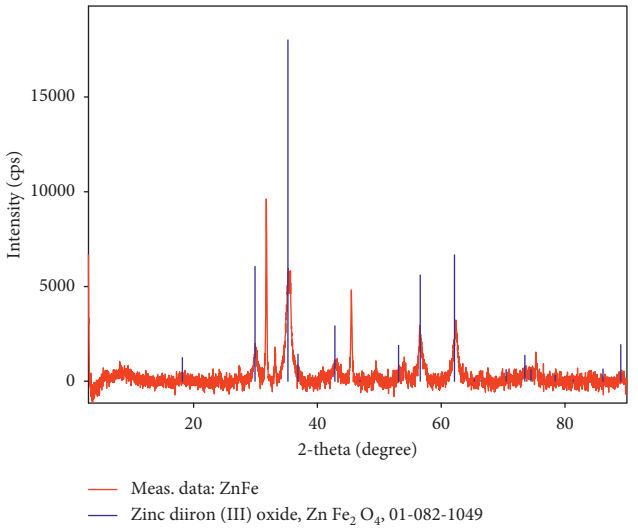

Figure 4: XRD spectrum of ZnF-based adsorbent before adsorption.

removal (Figure 1(b)). Also, from the images, the color removal mechanism is determined as adsorption (agglomerate sizes are about 30 nm and form large structures by connecting to each other) [14].

3.1.2. FTIR Analysis Results. FT-IR analyses were performed to determine the adsorption mechanism of ZnF adsorbent before and after dye adsorption. FTIR studies were conducted to detect the functional organic groups in the adsorbent at a frequency range of 500–4000 cm^{-1}, and Figures 2 and 3 display FTIR spectra of ZnF-based nanomaterials before and after AB 29 dye adsorption.

From Figure 2, it is seen that wide peak of O-H represents stretching vibration at 3450 cm^{-1} and the sharp peak at 500–600 cm^{-1} for Fe-O bond. The slight peak at 1625 cm^{-1} represents OH tension in molecular water. After dye adsorption (Figure 3), a slight peak shifts are observed at all peak ranges as a result of AB 29 adsorption of dye. Also, as a result of AB 29 adsorption of, it is seen that there is an alkoxy C-O bond at 1100 cm^{-1}.

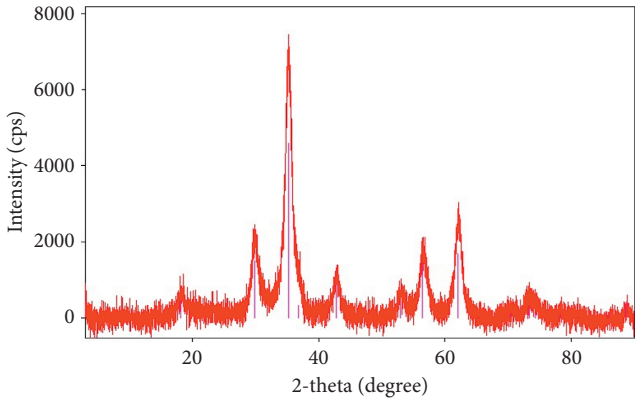

Figure 5: XRD spectrum of ZnF-based adsorbent after AB 29 dye adsorption.

Table 1: The adsorbed dye amount per unit adsorbent mass and removal values % at different initial pH values for AB 29 adsorption to ZnF-based nanomaterials.

pH	q_d (mg·g^{-1})	Removal %
2	98.83 ± 0.97	98.83
3	78.71 ± 0.45	78.71
4	8.74 ± 0.13	8.74
5	2.04 ± 0.03	2.04
6	3.49 ± 0.57	3.49
7	0.58 ± 0.06	0.58
8	1.16 ± 0.12	1.16
9	0.29 ± 0.04	0.29
10	0 ± 0	0

3.1.3. XRD Analysis Results. XRD analysis was carried out to investigate the phases and crystal structure of ZnF-based adsorbent used in AB 29 adsorption. The spectra of the XRD analysis (Figures 4 and 5) are shown below.

From the XRD analysis result, ZnF-based nanomaterials had a cubic crystal structure, and the impurity in the material did not change the cubic crystal structure as shown in Figures 4 and 5 [15]. XRD analysis proved that the simple formula of the material is $ZnFe_2O_4$.

3.2. Batch Adsorption Studies

3.2.1. Initial pH Effect and Isoelectric Point Effect. Initial pH is the most important parameter for color removal from wastewater. In this study, in order to observe the effects of pH parameter on AB 29 adsorption by ZnF-based nanomaterials, pH value was changed between 2.0 and 10.0 range as the initial dye concentration, and temperature and the adsorbent dosage were held constant at 100 mg·L^{-1}, 25°C and 1 g·L^{-1}, respectively.

The adsorbed dye per unit adsorbent mass and removal values % at different initial pH values for adsorption of AB 29 are shown in Table 1.

From Table 1, the favorable pH value for the highest removal efficiency is determined as 2.0. This phenomenon can be explained with isoelectric point. The adsorbent surface was loaded with a positive charge at pH values lower than the determined isoelectric point (pH = 7). Therefore, the electrostatic interaction between the positively charged adsorbent and the dyestuff anions has increased, and as a result, the adsorption capacity of the adsorbent has also increased.

3.2.2. Effect of Initial Dye Concentration. The effect of initial AB 29 dye concentrations on the adsorption by ZnF-based nanomaterials was investigated at an initial pH value of 2.0, temperature of 35°C, and adsorbent concentration of 1.0 g·L^{-1} in the range of 25–2000 mg·L^{-1} dye concentration. From the experimental results, when the initial dye concentration was increased from 25 mg·L^{-1} to 2000 mg·L^{-1} in AB 29 dye adsorption, the adsorbed dye amount in the unit adsorbent mass increased from 25 mg·g^{-1} to 1489.79 mg·g^{-1}, respectively. In AB 29 adsorption process, complete removal was observed at 300 minutes at initial dye concentration of 25 mg·L^{-1}, whereas the adsorption system was observed to reach the equilibrium at 1500 minutes at higher initial dyestuff concentrations.

3.2.3. Temperature Effect. The effect of temperature on the adsorption of AB 29 dye onto ZnF-based nanomaterials was investigated in the AB 29 concentration range and the temperature range of 25–2000 mg·L^{-1} and 25–55°C, respectively, by keeping the initial pH value constant at 2.0, adsorbent concentration of 1.0 g·L^{-1}.

The maximum amount of adsorbed dye per unit adsorbent mass for the adsorption of AB 29 at different temperature values for the equilibrium are shown in Table 2.

According to Table 2, as the temperature increases, there is an increase in adsorbed amounts per unit mass of adsorbent at equilibrium at high concentration levels. From the experimental results, maximum amounts of adsorbed dye per unit ZnF nanoparticle mass were observed at 35°C at high dye concentrations.

When the temperature is increased more than 55°C, the amount of adsorbed dye at equilibrium decreases due to some changes (loss of adsorbent surface activity resulting from temperature degradation of the adsorbent surface) originated in the interior structure of the adsorbent and affect the adsorption yield. This can be attributed to the loss of activity of the adsorbent surface by temperature increase and the degradation of some active sites on the surface by temperature.

3.3. The Effect of Adsorbent. Table 3 shows the effect of the adsorbent concentration on the adsorption of AB 29 by keeping constant the solution pH value of 2.0, initial dye concentration of 100 mg·L^{-1}, and the temperature of 25°C, when the adsorbent concentration are changed from 0.2 to 3.0 g·L^{-1}.

As seen from Table 3, the amount of adsorbed AB 29 by the unit mass of the adsorbent decreases with the increasing adsorbent dose. This is caused that the interaction of the adsorbent particles and agglomeration when the adsorbent dose is increased. From the same table, it is seen that the

Table 2: The maximum amount of dye adsorbed per unit adsorbent mass at different initial temperatures for the adsorption of the AB 29 dye onto ZnF-based nanomaterials.

C_0 (mg·L^1)	q_{max} (mg·g^{-1})			
	25°C	35°C	45°C	55°C
25	25 ± 0	24.56 ± 0.32	24.56 ± 0.28	24.27 ± 0.36
50	49.56 ± 0.19	48.83 ± 0.49	48.25 ± 0.73	48.83 ± 0.58
75	73.39 ± 1.39	72.52 ± 1.90	71.06 ± 1.32	71.64 ± 2.26
100	98.83 ± 0.97	94.75 ± 2.43	89.21 ± 1.36	92.41 ± 2.30
200	154.22 ± 1.95	164.43 ± 2.68	163.84 ± 2.27	150.14 ± 3.44
300	196.79 ± 3.86	219.53 ± 6.56	195.04 ± 3.22	185.13 ± 2.95
400	289.21 ± 4.92	300.87 ± 9.96	271.72 ± 6.69	245.48 ± 3.85
500	371.72 ± 10.17	376.96 ± 19.3	325.65 ± 6.71	285.42 ± 3.99
750	405.97 ± 6.47	557.58 ± 6.21	480.32 ± 17.73	411.80 ± 20.92
1000	755.10 ± 18.90	790.08 ± 12.64	526.23 ± 10.54	537.90 ± 20.58
1500	1132.65 ± 35.29	1155.97 ± 37.06	931.48 ± 21.62	736.15 ± 23.49
2000	1489.79 ± 47.06	1568.51 ± 53.39	1227.40 ± 49.51	976.67 ± 26.48

Table 3: The amount of dye adsorbed per unit mass of the adsorbent and the removal values % at different adsorbent concentrations for adsorption of AB 29 onto ZnF-based nanomaterials.

	AB 29 dye	
X_o (g·L^{-1})	q_d (mg·g^{-1})	Removal %
0.2	164.72 ± 0.34	17.99
0.5	137.01 ± 2.04	43.51
1.0	98.83 ± 0.97	82.00
2.0	49.84 ± 0.87	97.69
3.0	33.33 ± 0	98.53

increase of the adsorbent dose increases the adsorption yield, and it is observed that the color removal is detected as 98.53%, when the amount of adsorbent is 3 g in 1 L.

3.4. Adsorption Equilibrium. In this part of the investigation, linear regression, the best known conventional approach, is used for the determination of the isotherm parameters. For this purpose, Langmuir, Freundlich, and Tempkin isotherm models using the linear transform model (LTFM) are examined. The isotherm constant values are determined from the slope and intercept of the plots of each model equation in linear form. The isotherm parameters for each isotherm model are demonstrated in Table 4 [16, 17].

3.4.1. Langmuir, Freundlich, and Temkin Isotherm Models. Langmuir, Freundlich, and Temkin isotherm model constants were calculated from the plot of each model using the linear transform model (LTFM) and the determined constants and R^2 values are given in Table 4.

As it seen from Table 4, the R^2 values of Langmuir and Frendlich Isotherm models applied to AB 29-ZnF equilibrium data are quite high. According to linear transform model constants, it is determined that AB 29-ZnF adsorption equilibrium data are compatible with the Langmuir and Freundlich isotherm model. When Temkin model regression coefficients are examined for the AB 29 adsorption, it is seen that R^2 values are quite low, so the adsorption system seems to be incompatible with the Temkin model.

Table 4: Langmuir, Freundlich, and Temkin isotherm model constants with regression (R^2) coefficient values.

Langmuir Model				
T (°C)	25	35	45	55
Q° (mg·g^{-1})	303.03	285.71	217.39	277.77
b (L·mg^{-1})	0.4125	0.204	0.273	0.139
R^2	0.841	0.956	0.901	0.946
R_L	0.023	0.046	0.035	0.066
Freundlich Model				
T	25°C	35°C	45°C	55°C
$1/n$	0.3909	0.52	0.47	0.43
n	2.55	1.89	2.09	2.31
K_f ((mg/g)/(L/mg)$^{1/n}$)	13756.25	4138.09	3057.03	3478.56
R^2	0.817	0.937	0.958	0.955
Temkin Model				
T	25°C	35°C	45°C	55°C
A_t (L/g)	0.934	0.77	0.70	0.73
B (J/mol)	291.85	357.42	273.38	220.71
R^2	0.469	0.566	0.603	0.669

3.5. Adsorption Kinetics. In order to investigate the kinetic mechanism of the AB 29-ZnF-based nanoparticle adsorption system, the compatability of the experimental data obtained at different initial dye concentrations to the pseudo-first-order and pseudo-second-order kinetic models was examined [18]. For this purpose, log (q_d–q_t) values versus time graphs for AB 29 dye were plotted, and model rate constants and R^2 (regression coefficient) values from the linearized graph were obtained.

3.5.1. Pseudo-First-Order and Pseudo-Second-Order Kinetic Models. The pseudo-first-order kinetic model parameters obtained for the adsorption of the AB 29-ZnF system are presented in Table 5 with R^2 (regression coefficient) values. From the table, it is seen that the conformity of theoretical values to the experimental ones prove that the adsorption process is not presented with the pseudo-first-order kinetic model.

The pseudo-second-order kinetic model is used to investigate the kinetic mechanism of the AB 29-ZnF adsorption system, and kinetic model rate constants and R^2

Table 5: Pseudo-first-order kinetic model constants and R^2 (regression coefficient) values for adsorption of AB 29 dye on ZnF-based nanomaterials.

C_o (mg·L^{-1})	$q_{d,experimental}$	$q_{d,calculated}$	k_1 (min^{-1})	R^2
25	25	14.77	0.016812	0.963
50	49.56	44.08	0.010824	0.977
75	73.39	61.91	0.006679	0.993
100	98.83	102.42	0.009212	0.991
200	154.22	149.27	0.003455	0.975
300	196.79	214.68	0.003915	0.958
400	289.21	313.40	0.002994	0.979
500	371.72	357.35	0.002533	0.988
750	405.97	363.07	0.003685	0.930
1000	755.10	889.61	0.003915	0.988
1500	1132.65	1249.97	0.002994	0.983
2000	1489.79	1842.46	0.003685	0.985

(regression coefficient) values were determined from the graph of t/q_t versus time at different AB 29 concentrations, as presented in Table 6 [19].

The pseudo-second-order kinetic model supposed that the rate limiting step includes chemisorption of adsorbate on the adsorbent. From Table 6, at all concentrations, pseudo-second-order linear regression correlation coefficients (R^2) were much higher than those of the pseudo-first-order model, and the conformity of theoretical values with the experimental ones prove that adsorption process cannot be represented by the pseudo-first-order kinetic model. This proved that the ZnF adsorption kinetics of AB 29 was not diffusion-controlled [20].

3.6. Adsorption Thermodynamics. Thermodynamic parameters such as Gibbs Free energy change (ΔG), enthalpy change (ΔH), and entropy change (ΔS) values were evaluated according to the Van't Hoff equation to investigate the effect of temperature on the adsorption of AB 29 by ZnF-based nanomaterials [21]. Gibbs free energy change (ΔG), enthalpy change (ΔH), and entropy change (ΔS) values calculated from thermodynamic equations are presented in Table 7.

As it seen from Table 7, the values of Gibbs free energy change (ΔG), enthalpy change (ΔH), and entropy change (ΔS) terms are negative for the AB 29-ZnF adsorption system. This shows that the adsorption process for the AB 29-ZnF system is exothermic ($\Delta H < 0$), spontaneous ($\Delta G < 0$), and stabilized ($\Delta S < 0$) without structural change at the solid/liquid interface [22, 23]. Purkait et al. [24], Iqbal and Ashiq [25], and Karaoğlu et al. [26] have obtained similar thermodinamically adsorption behaviour results in their own investigations.

3.7. Determination of Antimicrobial Effect of Adsorbent. When the literature is reviewed, it is found that ZnF-based nanomaterials have high antimicrobial property. This part of the investigation is related with the determination of the antimicrobial effect of the ZnF-based nanoadsorbent.

In this experimental part, the antimicrobial properties of ZnF-based nanomaterials produced by the hole agar diffusion method were determined by the cavity diffusion

Table 6: Pseudo-second-order kinetic model constants and R^2 (regression coefficient) values for adsorption of AB 29 dye on ZnF-based nanomaterials.

C_0 (mg·L^{-1})	$q_{d,experimental}$	$q_{d,calculated}$	k_2 (g·mg^{-1}·min^{-1})	R^2
25	25	25.12	0.006346	1.00
50	49.56	50.50	0.000736	0.999
75	73.39	75.18	0.000288	0.999
100	98.83	102.04	0.000183	0.998
200	154.22	166.66	4E–05	0.998
300	196.79	212.76	2.67E–05	0.986
400	289.21	333.33	1.01E–05	0.962
500	371.72	416.66	9.52E–06	0.964
750	405.97	476.19	7E–06	0.982
1000	755.10	1000	2.18E–06	0.953
1500	1132.65	1428.57	1.93E–06	0.9538
2000	1489.79	2500	4.19E–07	0.8654

Table 7: Thermodynamic parameters calculated from the Van't Hoff equation for adsorption of AB 29 dyes on ZnF-based nanomaterials.

T (K)	ΔG (J·mol^{-1})	ΔH (kJ·mol^{-1})	ΔS (J·mol·K^{-1})	$T\Delta S$ (J·mol^{-1})
298	−16704.5			−75536.1
308	−13305.6	−91.96	−253.48	−78070.9
318	−11673.3			−80605.7

methodology with two different Gram-positive (*Bacillus subtilis* and *Enterococcus fecalis*) and two Gram-negative (*Escherichia coli* and *Klebsiella pneumoniae*) bacteria. The inhibition areas observed as a result of the diffusion susceptibility test are presented in Table 8. The inhibition areas observed for *Bacillus subtilis*, *Enterococcus fecalis*, *Escherichia coli*, and *Klebsiella pneumoniae* bacteria with the susceptibility test are shown in Table 8 (field area size) and in Figure 6 (images).

From the experimental results, it can be said that ZnF-based nanomaterials have antimicrobial property to the antimicrobial effect of four different bacteria at various adsorbent doses. When the experimental data was evaluated, it was seen that the inhibition zones were observed at 25 mg/

Table 8: The inhibition fields observed as a result of the diffusion susceptibility test.

Type of bacteria	Amount of substance (mg·mL^{-1})	Inhibition field diameter (mm)
Bacillus subtilis	25	—
	50	11
	75	15
Enterococcus fecalis	25	—
	50	13
	75	18
Escherichia coli	25	14.5
	50	18
	75	21
Klebsiella pneumoniae	25	—
	50	10
	75	16.5

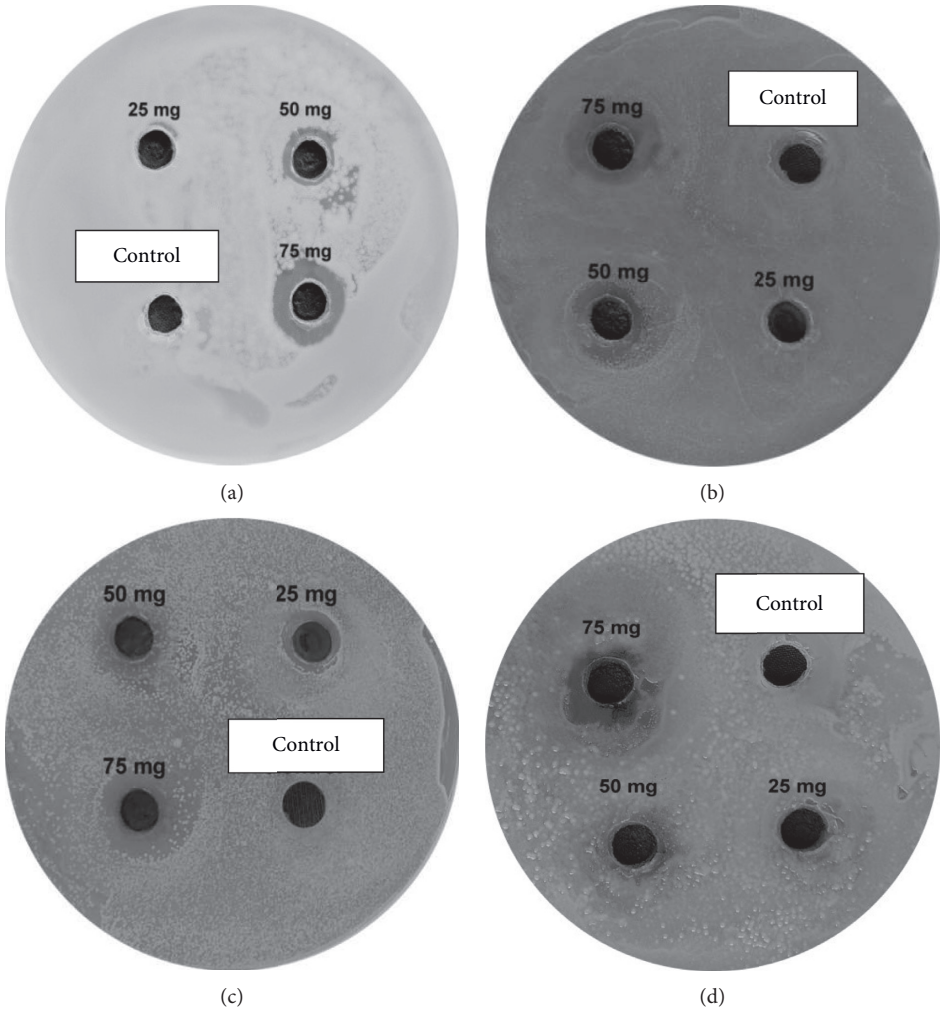

Figure 6: Determination of the antimicrobial effect of ZnF-based nanomaterials on (a) *Bacillus subtilis*, (b) *E. fecalis*, (c) *E. coli*, and (d) *K. Pneumoniae* by the diffusion susceptibility method.

L, 50 mg/L, and 75 mg/L dosages for *E. coli*; at 50 mg/L and 75 mg/L dosages for *Bacillus subtilis* and *Enterococcus fecalis bacteria*; and at 75 mg/L dosage for *Klebsiella pneumoniae bacteremia*.

As a result of the experimental studies, ZnF-based nanomaterials have superior advantage of advanced antimicrobial property against many harmful pathogens besides ecofriendly color removal [26–29].

4. Conclusion

In this investigation, the adsorption of AB 29 dye onto ZnF-based nanomaterials was experimentally researched in a batch system. ZnF-based nanomaterials were synthesized by the coprecipitation method and used for the adsorption of AB 29 dye solution. For the particle characterization, FT-IR was used to identify functional groups in the characterization of the obtained nanomaterials. XRD was used for crystal structure and phase analysis; SEM analyses were performed for surface morphology. As a result of these analyzes, color removal mechanism for the AB 29-ZnF system was determined as adsorption, and the simple formula of the material is detected as $ZnFe_2O_4$. From the antimicrobial effect determination experiments for antimicrobial effect of ZnF-based nanomaterials, it is proved that nanomaterials have advanced antimicrobial property for two different Gram-positive (*Bacillus subtilis* and *Enterococcus fecalis*) and two Gram-negative (*Escherichia coli* and *Klebsiella pneumoniae*) bacteria.

In the other part of the studies, Langmuir, Freundlich, and Temkin isotherm models were applied to the adsorption equilibrium data obtained at different temperatures in the adsorption of AB 29 dye solution onto ZnF-based nanomaterials. It was observed that the equilibrium data of the adsorption process was very compatible with the Langmuir and Freundlich isotherm models.

In order to examine the adsorption kinetics, the kinetic models in the literature were applied to the experimental data for adsorption system. The adsorption data results indicated that the pseudo-second-order kinetic model fitted well the adsorption data of AB 29 onto the ZnF nanoparticles, and it was concluded that the rate limiting step would be chemisorption.

Thermodynamic parameters such as Gibbs free energy change (ΔG), enthalpy change (ΔH), and entropy change (ΔS) were calculated according to the Van't Hoff equation with the help of data obtained at different temperatures. According to experimental results, the AB 29-ZnF system is exothermic ($\Delta H < 0$), spontaneous ($\Delta G < 0$), and stabilized ($\Delta S < 0$) without structural change at the solid/liquid interface.

As a result of the experimental investigation carried out, ZnF-based nanomaterials have superior advantages such as environmental friendliness, antimicrobial character against many harmful pathogens, and simplicity of the synthesis procedure.

In this research, removal of single pollutant (AB 29 textile dye) from synthetically prepared wastewater was investigated by using a novel adsorbent ($ZnFe_2O_4$). However, many different pollutants (heavy metals, phenol, phosphorus, oil, etc.) can be found together in domestic or industrial wastewater at the same time. Thus, taking into account the effects of more than one pollutant, large scale experimental studies for treatment of actual wastewater systems can be achieved. In addition, this study can be proceeded with the help of using a continuous system or more than one reactor to serve the purpose for the high dye removal percentages and reduction of equilibrium time.

Conflicts of Interest

The authors report no conflicts of interest.

Acknowledgments

This investigation was financially sponsored by Mersin University Research Fund Project no. 2017-1-TP2-2266. The authors thank "Mersin University, Department of Scientific Research Projects" "Advanced Technology Education Research and Application Center" for the characterization of the nanoparticle and Dr. A.O. Adıgüzel from Faculty of Science, Biology Department, Mersin University, for the help of the determination for antimicrobial activity of the nanoparticle.

References

[1] J. Rajeev and M. Shrivastava, "Photocatalytic removal of hazardous dye cyanoise from industrial watse using titanium dioxide," *Journal of Hazardous Materials*, vol. 152, pp. 216–220, 2008.

[2] C. C. Chen, A. J. Chaudhary, and S. M. Grimes, "Photodegradation of acid blue 29 and ethyl violet in the presence/absence of sodium hydroxide and aluminum ions," *Journal of Hazardous Materials*, vol. 117, pp. 171–178, 2005.

[3] D. R. Acosta, A. I. Martinez, A. A. Lopez, and C. R. Magana, "Titanium dioxide thin films: the effect of the preparation method in their photocatalytic properties," *Journal of Molecular Catalysis A: Chemical*, vol. 228, no. 1-2, pp. 183–188, 2005.

[4] A. Denizli, R. Say, and Y. Arica, "Removal of heavy metal ions from aquatic solutions by membrane chromatography," *Separation and Purification Technology*, vol. 21, no. 1-2, pp. 181–190, 2000.

[5] S. Arica and V. Singh, "TiO_2 mediated photocatalytic degradation studies of reactive red 198 by UV irradiation," *Journal of Hazardous Materials*, vol. 141, no. 1, pp. 230–236, 2007.

[6] I. A. Alaton, I. A. Balcioglu, and D. W. Bahnemann, "Advanced oxidation of a reactive dyebath effluent: comparison of O_3, H_2O_2/UV-C and TiO_2/UV-A processes," *Water Research*, vol. 36, no. 5, pp. 1143–1154, 2002.

[7] U. Pagga and D. Brown, "The degradation of dyestuffs: part II behaviour of dyestuffs in aerobic biodegradation tests," *Chemosphere*, vol. 15, no. 4, pp. 479–491, 1986.

[8] A. Mittal, J. Mittal, and L. Kurup, "Adsorption isotherms, kinetics and column operations for the removal of hazardous dye, tartrazine from aqueous solutions using waste materials—bottom ash and de-oiled soya, as adsorbents," *Journal of Hazardous Materials*, vol. 136, no. 3, pp. 567–578, 2006.

[9] A. K. Singh, A. Mittal, J. Mittal, and L. Kurup, "Process development for the removal and recovery of hazardous dye erythrosine from wastewater by waste materials-bottom ash and de-oiled soya as adsorbents," *Journal of Hazardous Materials*, vol. 138, no. 1, pp. 95–105, 2006.

[10] V. K. Gupta, A. Mittal, L. Kurup, and J. Mittal, "Adsorption of a hazardous dye, erythrosine, over hen feathers," *Journal of Colloid and Interface Science*, vol. 304, no. 1, pp. 52–57, 2006.

[11] S. Mandal, S. Natarajan, A. Tamilselvi, and S. Mayadevi, "Photocatalytic and antimicrobial activities of zinc ferrite nanoparticles synthesized through soft chemical route: a magnetically recyclable catalyst for water/wastewater

treatment," *Journal of Environmental Chemical Engineering*, vol. 4, no. 3, pp. 2706–2712, 2016.

[12] L. Boyanova, G. Gergova, R. Nikolov et al., "Activity of Bulgarian propolis against 94 *Helicobacter pylori* strains in vitro by agar-well diffusion, agar dilution and disc diffusion methods," *Journal of Medical Microbiology*, vol. 54, no. 5, pp. 481–483, 2005.

[13] S. Alpdoğan, A. O. Adıgüzel, B. Sahan, M. Tunçer, and H. M. Gubur, "Effects of bacteria on CdS thin films used in technological devices," *Materials Research Express*, vol. 4, no. 4, p. 46402, 2017.

[14] R. Sivaraj, P. K. S. M. Rahman, P. Rajiv, H. A. Salam, and R. Venckatesh, "Biogenic copper oxide nanoparticles synthesis using *Tabernaemontana divaricate* leaf extract and its antibacterial activity against urinary tract pathogen," *Spectrochimica Acta Part A: Molecular and Biomolecular Spectroscopy*, vol. 133, pp. 178–181, 2014.

[15] P. Logeswari, S. Silambarasan, and J. Abraham, "Synthesis of silver nanoparticles using plants extract and analysis of their antimicrobial property," *Journal of Saudi Chemical Society*, vol. 19, no. 3, pp. 311–317, 2015.

[16] W. Konicki, D. Sibera, E. Mijowska, Z. Lendzion-Bieluń, and U. Narkiewicz, "Equilibrium and kinetic studies on acid dye acid red 88 adsorption by magnetic $ZnFe_2O_4$ spinel ferrite nanoparticles," *Journal of Colloid and Interface Science*, vol. 398, pp. 152–160, 2013.

[17] C. Muthukumaran, V. M. Sivakumar, and M. Thirumarimurugan, "Adsorption isotherms and kinetic studies of crystal violet dye removal from aqueous solution using surfactant modified magnetic nanoadsorbent," *Journal of the Taiwan Institute of Chemical Engineers*, vol. 63, pp. 354–362, 2016.

[18] Y. E. Boundati, K. Ziat, A. Naji, and M. Saidi, "Generalized fractal-like adsorption kinetic models: application to adsorption of copper on Argan nut shell," *Journal of Molecular Liquids*, vol. 276, pp. 15–26, 2019.

[19] F. Gimbert, N. Morin-Crini, F. Renault, P.-M. Badot, and G. Crini, "Adsorption isotherm models for dye removal by cationized starch-based material in a single component system: error analysis," *Journal of Hazardous Materials*, vol. 157, no. 1, pp. 34–46, 2008.

[20] Y.-J. Tu, C.-F. You, and C.-K. Chang, "Kinetics and thermodynamics of adsorption for Cd on green manufactured nano-particles," *Journal of Hazardous Materials*, vol. 235-236, pp. 116–122, 2012.

[21] O. Długosz and M. Banach, "Kinetic, isotherm and thermodynamic investigations of the adsorption of Ag^+ and Cu^{2+} on vermiculite," *Journal of Molecular Liquids*, vol. 258, pp. 295–309, 2018.

[22] A. Afkhami, S. Sayari, R. Moosavi, and T. Madrakian, "Magnetic nickel zinc ferrite nanocomposite as an efficient adsorbent for the removal of organic dyes from aqueous solutions," *Journal of Industrial and Engineering Chemistry*, vol. 21, pp. 920–924, 2015.

[23] F. Zhang, X. Chen, F. Wu, and Y. Ji, "High adsorption capability and selectivity of ZnO nanoparticles for dye removal," *Colloids and Surfaces A: Physicochemical and Engineering Aspects*, vol. 509, pp. 474–483, 2016.

[24] S. Banerjee and M. C. Chattopadhyaya, "Adsorption characteristics for the removal of a toxic dye, tartrazine from aqueous solutions by a low cost agricultural by-product," *Arabian Journal of Chemistry*, vol. 10, pp. S1629–S1638, 2017.

[25] S. Haciyakupoglu, E. Orucoglu, A. N. Esen, S. Yusan, and S. Erenturk, "Kinetic modeling of selenium (IV) adsorption for remediation of contaminated aquatic systems based on meso-scale experiments," *Desalination and Water Treatment*, vol. 56, no. 5, pp. 1208–1216, 2015.

[26] M. K. Purkait, S. DasGupta, and S. De, "Adsorption of eosin dye on activated carbon and its surfactant based desorption," *Journal of Environmental Management*, vol. 76, no. 2, pp. 135–142, 2005.

[27] M. J. Iqbal and M. N. Ashiq, "Adsorption of dyes from aqueous solutions on activated charcoal," *Journal of Hazardous Materials*, vol. 139, no. 1, pp. 57–66, 2007.

[28] M. H. Karaoğlu, M. Doğan, and M. Alkan, "Kinetic analysis of reactive blue 221 adsorption on kaolinite," *Desalination*, vol. 256, pp. 154–165, 2010.

[29] A. R. Yari, S. Nazari, A. Rastegar, S. Alizadeh-Matboo, G. Majidi, and M. Tanhaye-Reshvanloo, "Removal of acid red 18 dye from aqueous solutions using nanoscale zero-valent iron," *Iranian Journal of Health Sciences*, vol. 3, no. 3, pp. 63–69, 2015.